1990MNRAS.245..470B

Mon. Not. R. astr. Soc. (1990) **245**, 470–483

Profiles of emission lines in active galactic nuclei – III. Observations of Hα, [N II] and [S II] profiles★

I. C. Busko† and J. E. Steiner

Department of Astrophysics, Instituto de Pesquisas Espaciais, Caixa Postal 515 - 12201 - São José dos Campos - SP - Brazil

Accepted 1990 March 9. Received 1990 February 19; in original form 1989 July 3

SUMMARY

High-resolution (FWHM = 28 km s^{-1}) observations of Hα, [N II] λ6548/6583 and [S II] λ6717/6731 emission lines in several southern active galactic nuclei (AGN) are presented. Deblending of the Hα + [N II] profiles was performed using, when available, the [O III] λ5007 profile shape as a template. Line profile measurements, as well as line intensities, are tabulated. We found to be relatively common among the observed objects the existence of structure in the line cores, pointing to the complexity of the dynamics in the low-velocity emission region. Differences in profile shape and width amongst different lines are also common, indicating that often there is a superposition, on the spectrograph slit, of emission regions with different dynamics and excitation conditions. This superposition is quantified in the case of IC 5063. We found weak, broad Hα emission in IC 5063 and IC 5135. In NGC 2992, we were unable to confirm the presence of a broad Hα component with the same intensity as found by previous authors, which we ascribe to spectral resolution effects.

1 INTRODUCTION

The study of emission-line profiles in Active Galactic Nuclei (AGN) has been a powerful tool in diagnosing the dynamical state of the emitting gas, as well as its spatial and ionization structure. As discussed in Busko & Steiner (1988, hereafter Paper I) and Busko & Steiner (1989a, hereafter Paper II), the main subject in observational studies of narrow line region (NLR) emission-line profiles has been the bright [O III] λ5007 line. However, studies of other emission lines, covering a range of ionization and excitation conditions, are a necessary step in the buildup of a consistent picture of the NLR structure.

Unfortunately, no statistical studies of the kind presented in Paper II, and references therein, are possible yet for emission lines other than [O III] λ5007. As shown in Paper II, if we restrict ourselves to observations with resolutions equal to or better than 130 km s^{-1}, we can find in the literature about 165 objects with measured [O III] profile shape data. For other emission lines, using the same resolution criterion, only the nine objects published by Whittle (1985b) (and the seven by Appenzeller & Östreicher 1988) can be counted on. Some recent data on individual objects (e.g. Ayani & Iye 1989) are not well-suited for purposes of comparison with other width and asymmetry data, due to the way the profiles were measured (Gaussian decomposition).

This fact led us to design an observational program aimed at obtaining AGN narrow line profile data, with high spectral resolution ($R = 10^4$) and moderate signal-to-noise ratio, and emphasizing bright lines other than [O III] λ5007. The observations were obtained with the 1.6-m telescope/coudé spectrograph combination of CNPq/Laboratório Nacional de Astrofísica (Brazil), using as detector a two-channel intensified photon-counting Reticon. Due to the relatively small telescope size, we restricted the program to the brightest southern AGN (Paper I). Also, due to limitations in detector sensitivity and spectral coverage, we restricted the observations to the strongest emission lines: Hα + [N II] λ6548/6583 (and [S II] λ6717/6731 included as a bonus), as well as [O III] λ4959/5007.

In Paper I we described in detail the observational and data reduction methods used, and reported the data secured for the [O III] λ4959/5007 lines. The aim of the present paper is to report the data on the other emission lines observed in the same program. Forthcoming Paper IV will present a comprehensive analysis of all the data obtained in the program.

2 OBSERVATIONS AND DATA REDUCTION

A journal of the Hα + [N II] and [S II] observations is presented in Table 1. Ionization class includes high (Sy) and low (LINER) subclasses. These, as well as galaxy type for each object, were taken from references in Paper II. The broad/

★Based on observations made at CNPq/Laboratório Nacional de Astrofísica, Brazil.

†Present address: Space Telescope Science Institute, 3700 San Martin Drive, Baltimore, MD 21218, USA.

© Royal Astronomical Society • Provided by the NASA Astrophysics Data System

1990MNRAS.245..470B

narrow Balmer line ratio classification is based on results of the present paper. Due to several causes, only a fraction of the objects were also observed in the [O III] + Hβ region. These causes, as well as the instrumental and data acquisition details of the observing program, were discussed in Paper I.

In three objects we found contamination in the detector sky channel. One case (NGC 7213) was already discussed in Paper I. The other two objects (NGC 253 and NGC 1097), however, showed noticeable *line* emission in an extended region around the visual nucleus. We did not subtract the sky spectrum in the reduction procedure, but simply measured the profile parameters on the raw spectra, treating the sky channel as a second object. These objects are discussed in detail in Section 3.

Fig. 1 shows the Hα + [N II] and [S II] line profiles, after reduction by the procedures described in Paper I, and after being rebinned to a linear velocity scale. In these and all subsequent spectral plots, the abscissa is velocity in the object reference frame and the ordinate is counts per 10 km s^{-1} velocity bin. We note that, due to the I-Ret image tube characteristics, the actual count rate on the [S II] region was less than indicated in Fig. 1. The values shown there result after flat-field division, and are useful for comparisons with count rates in the Hα region, but not for statistical evaluation.

The profile measuring techniques employed on the [O III] line were described in Paper I. However, both the Hα + [N II] and the [S II] lines show blending problems not found in the [O III] case, so we had to take added care in the measurement of those profiles.

With the spectral resolution used (28 km s^{-1} at 6600 Å), the main difficulty in treating the [N II] and narrow Hα profiles is the blending of the extreme line wings, as well as the possible superposition of a broad Hα line. Both effects can impair the baseline fitting to such an extent that the integral measuring method proposed by Whittle (1985a) for the [O III] line cannot be used at all. Instead, we restricted ourselves to measuring the profiles by the method of Heckman *et al.* (1981).

Before applying the technique described in Paper I to each individual narrow-line profile, we tried to minimize the blending problem by removing offending lines that lie close to a line of interest. In the case of Hα, we removed both [N II] λ6548 and λ6583. In the case of [N II] λ6583, we removed narrow Hα. In both cases, the remaining profile was cleaned of a broad Hα component, when necessary, by fitting to regions outside the remaining narrow lines an even-degree polynomial (usually 2nd or 4th degree). We did not measure [N II] λ6548 because its signal-to-noise is lower than in λ6583, and also because it lies closer to narrow Hα than [N II] λ6583 does, thus worsening the blending problem.

Two methods were used to remove the narrow neighbour profiles in the region Hα + N[II]: (i) when an [O III] profile was also observed for the same object, and when its shape approximately resembled that of N[II] and narrow Hα, it was used as a profile shape template. After removing its baseline, it was lightly smoothed by a triangular filter, multiplied by an arbitrary factor F and subtracted from the blended profile in velocity space. The value of F was varied until the smoothest residual was obtained. In the case of [N II] removal, both lines were removed simultaneously, their respective F values being constrained to the ratio 2.8; (ii) when no [O III] profile was available, we simply estimated by eye a baseline (approximated by a polynomial), which could include a broad Hα component, and used it to interpolate in the region(s) occupied by the unwanted line(s). This procedure is justifiable in most cases, since the narrow lines in these objects are relatively narrow and unblended and/or the estimated broad Hα line is relatively weak, or even undetectable. However, it is not satisfactory in the case of NGC 5728, where highly structured and blended narrow lines are seen. Results for this object must be taken as approximate only.

In the first procedure outlined above, it can be argued that since differences beween narrow-line profiles in the same object are known in several cases, it is not always valid to use one given line as a shape template for another one. In fact, in some cases it was difficult to decide when the 'smoothest' residual was reached, due to these profile differences. In order to get an estimate for the error in the profile parameters introduced by this deblending procedure, we analysed three objects, chosen on the basis of their Hα broad/narrow intensity ratio (F51, IC 5135 and IC 5063), with the following procedure. First, we created for each object two new deblended spectra, using F values 10 per cent, respectively, below and above the one that generated the 'smoothest' residual. In these new deblended spectra, the under/over deblending correction error, in the form of a residual bump/depression in the regions around -680 and $+960$ km s^{-1}, was small but clearly visible. This showed that F can be estimated with an accuracy better than 10 per cent in most cases. We next measured the resulting spectra with the techniques described in Paper I.

The variations between profile parameters (widths, asymmetries) coming from over- and under-corrected

Table 1. Journal of observations.

Object	Ioniz.[a] class	AGN class	Galaxy type	Date	Exp. (min.)	P.A.[b] (deg.)
NGC 253	L	2	SBc	08/05/85	50	136
				08/05/85	125	107
				09/05/85	60	122
NGC 1052	L	1.5	E	04/10/85	55	117
NGC 1097	L	2	SB	24/08/85	78	117
				06/09/85	57	130
NGC 1566	Sy	1.9[c]	Sb-c	04/10/85	55	132
NGC 2992	Sy	2	Sa	13/03/85	95	102
NGC 5728	Sy	2 (?)	SB(r)	04/08/85	130	63
NGC 6300	L?	2	SBc	23/08/85	267	135
NGC 6814	Sy	1.2	Sb	20/07/84	120	82
NGC 7213	L	1.5	E	18/07/84	200	138
NGC 7552	Sy	2	S	22/08/85	50	141
NGC 7582	Sy	2	SB(r)	22/08/85	60	117
IC 4329A	Sy	1-1.2	S	11/05/85	80	119
IC 5063	Sy	1.9	S0-a	19/07/84	120	130
IC 5135	Sy	2 (1.9?)	Sb	14/05/85	96	155
				04/08/85	44	107
Mkn 926	Sy	1	E	24/08/85	125	120
Mkn 938	Sy	2	inter.	03/10/85	140	113
F9	Sy	1.2	S	17/07/84	100	169
F51	Sy	1.2	S	17/07/84	160	175
ESO141-G55	Sy	1-1.2	SBc	16/07/84	120	174
MCG-6-30-15	Sy	1.2	S	19/07/84	120	80

Notes: [a]L – low ionization; Sy – high ionization; [b]position angle at mid-exposure; [c]at this particular observation, see text.

© Royal Astronomical Society • Provided by the NASA Astrophysics Data System

1990MNRAS.245..470B

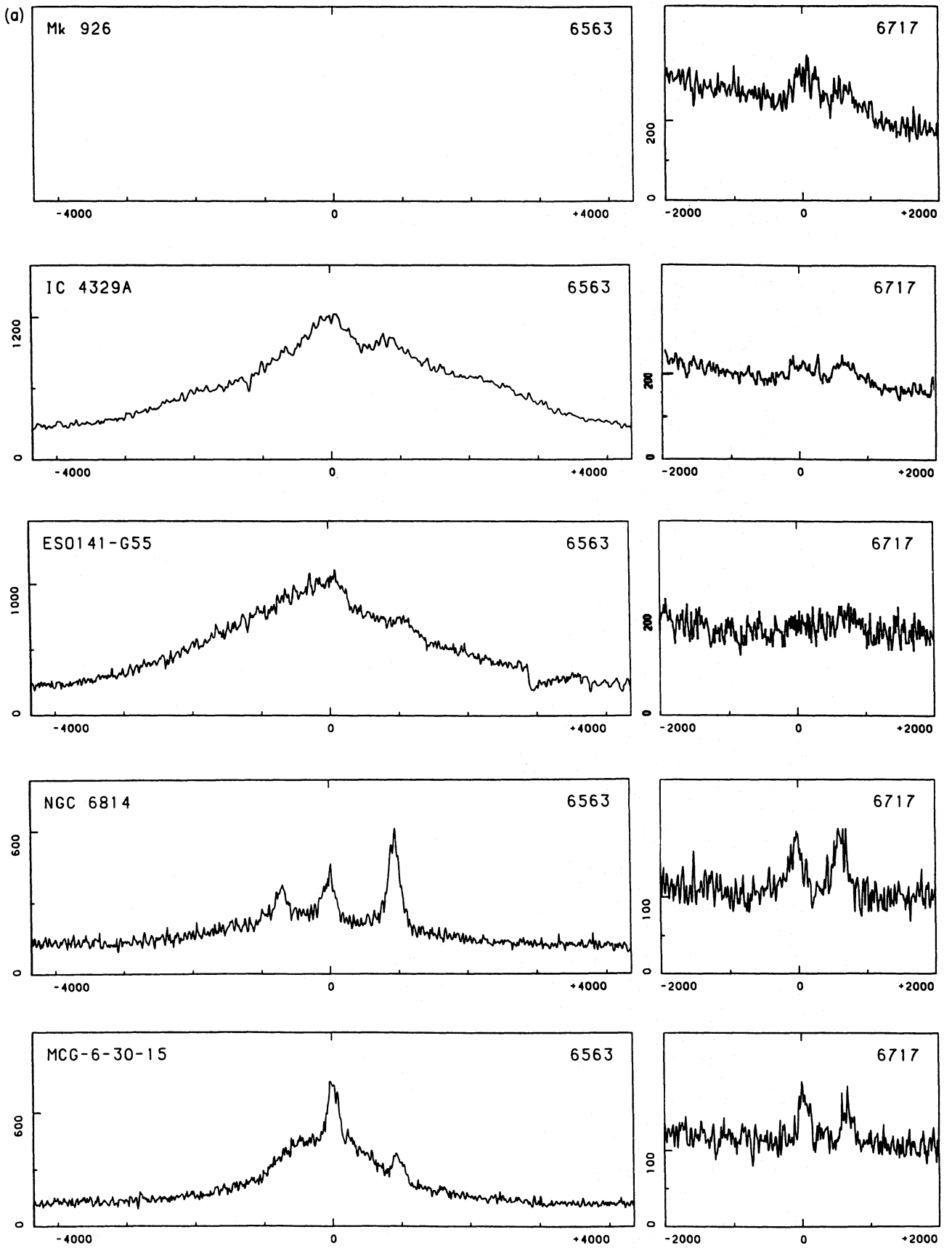

Figure 1. Hα + [N II] λ6548/6583 (left panel) and [S II] λ6717/6731 (right panel) emission-line profiles. Abscissa: velocity (in km s^{-1}) in the object reference frame. reference wavelength is shown in the upper right of each panel. Ordinate: total counts per 10 km s^{-1} velocity bin. Data for Mk 926 are absent due to obliteration by O_2 band at λ6870.

© Royal Astronomical Society • Provided by the NASA Astrophysics Data System

1990MNRAS.245..470B

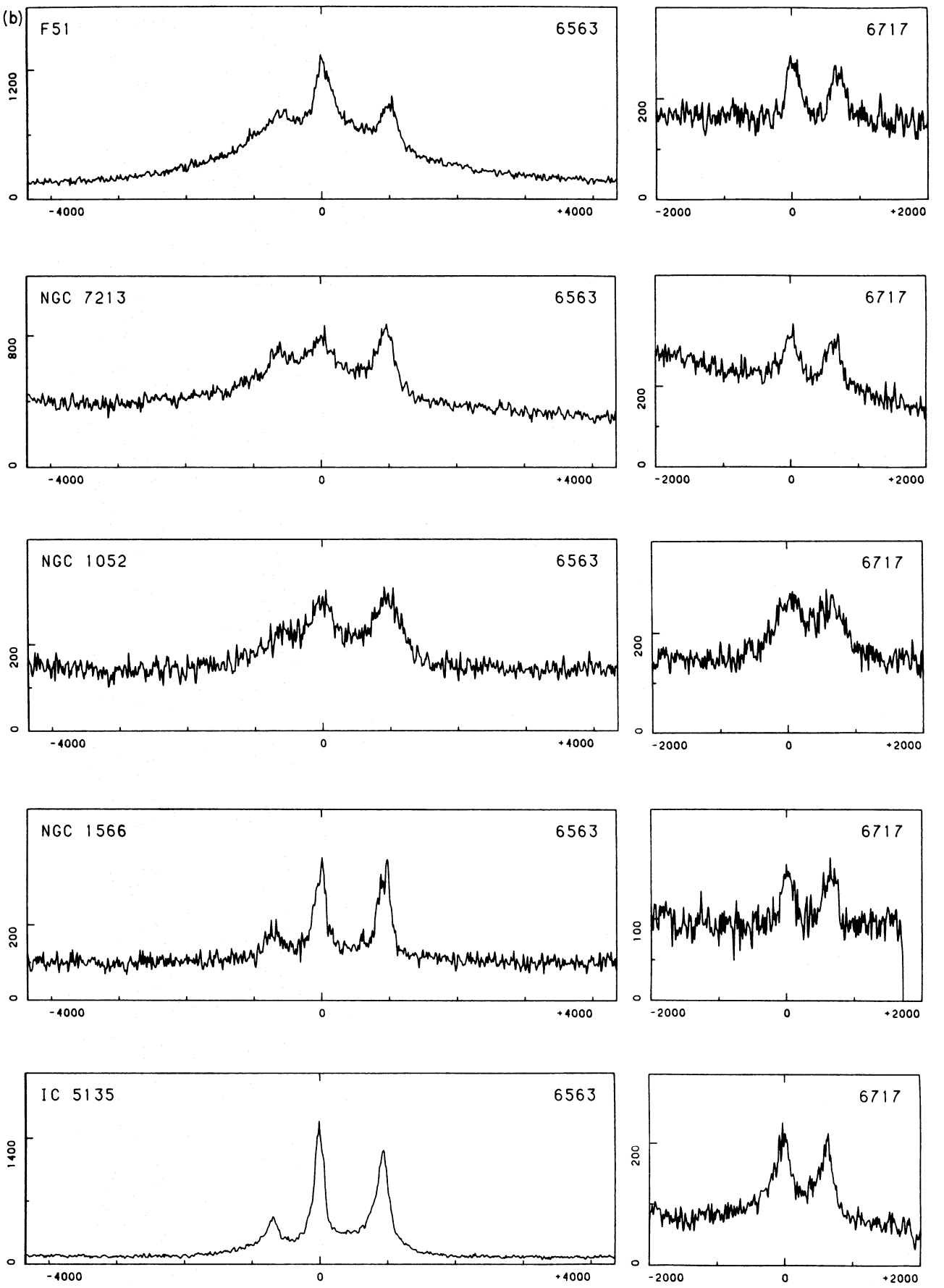

Figure 1 – *continued*

© Royal Astronomical Society • Provided by the NASA Astrophysics Data System

1990MNRAS.245..470B

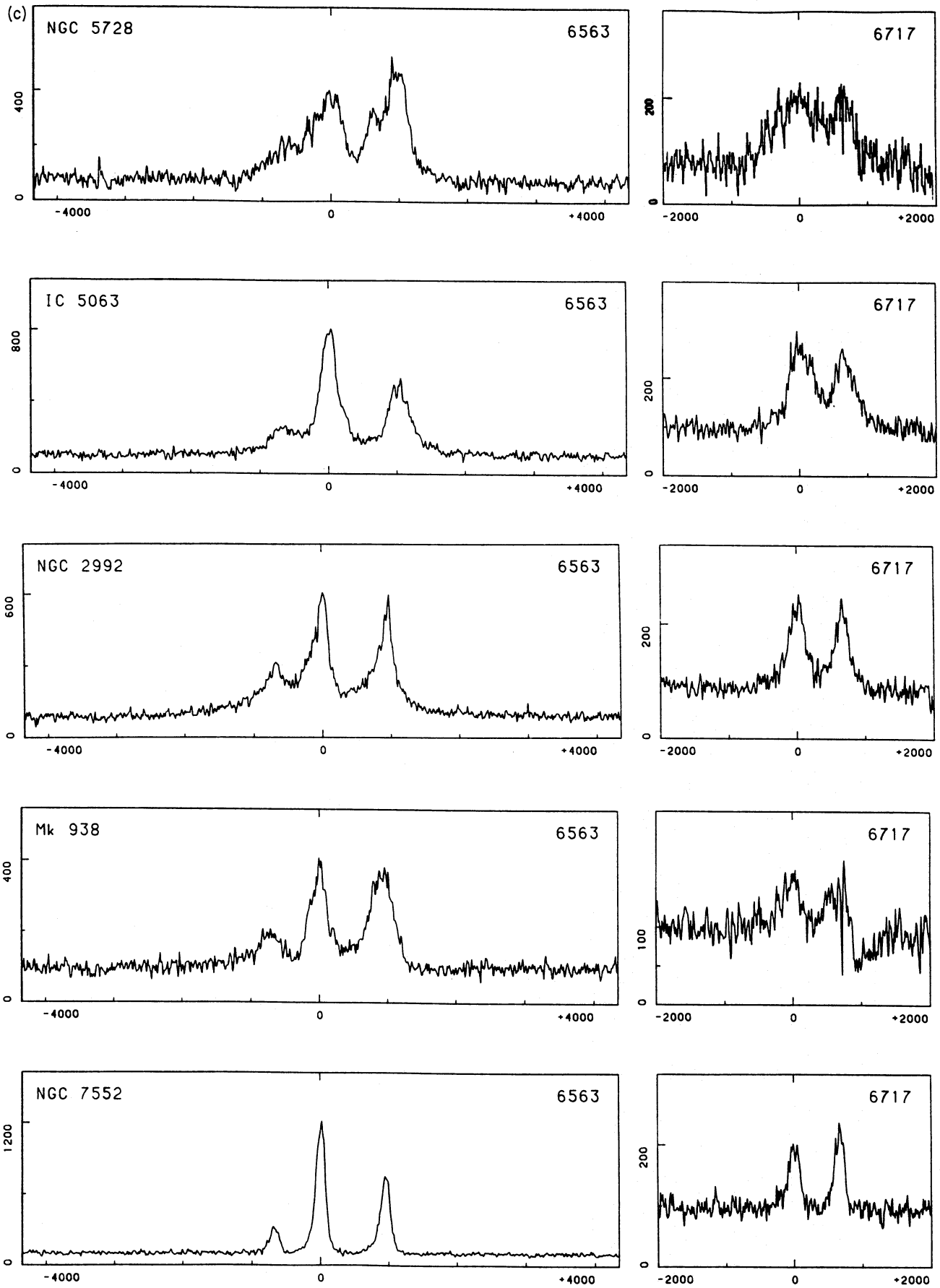

Figure 1 – *continued*

© Royal Astronomical Society • Provided by the NASA Astrophysics Data System

1990MNRAS.245..470B

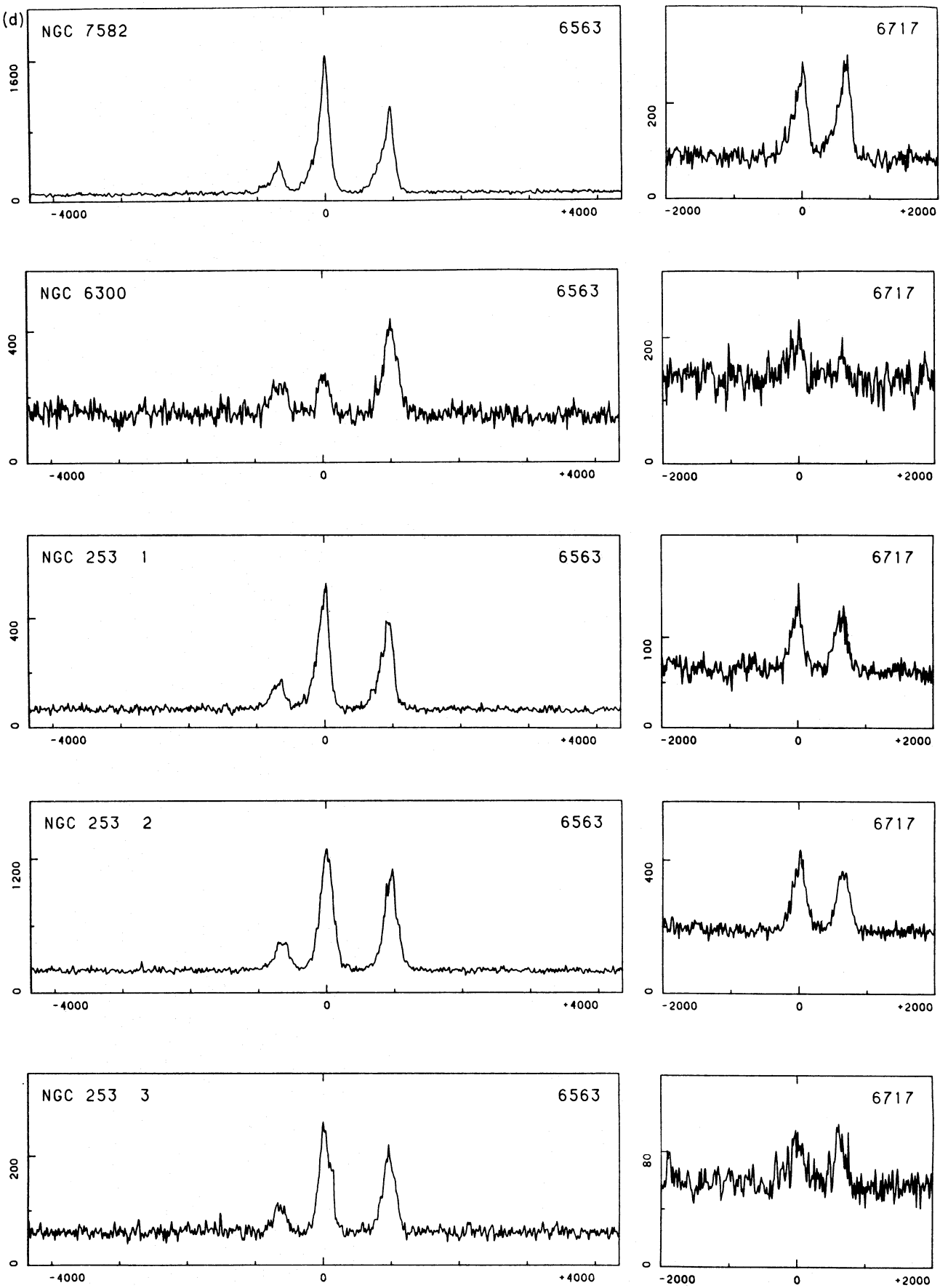

Figure 1 – *continued*

© Royal Astronomical Society • Provided by the NASA Astrophysics Data System

1990MNRAS.245..470B

spectra were always of the same order or smaller than the formal errors of the same parameters, for all fractional levels above the 10 per cent one. For this fractional level the variations in profile parameters were significantly greater than the parameters' formal errors, showing that the deblending procedure introduced a greater amount of error in the extreme line wings, as expected. Also, the variation in the equivalent width (see below) of the Hα narrow and broad components was of the order of 5–10 per cent, except in the case of the broad component in IC 5063, in which the equivalent width variation was 35 per cent. This is understandable since this object has a relatively weak broad Hα component. According to these results, we did not attempt to measure zero-height parameters for the lines studied here, as was done in Paper I for the [O III] line. The 10 per cent parameters presented here must be taken as approximations only. In particular, formal errors assigned to them do not include the extra uncertainty introduced by the deblending process.

Problems similar to the ones found with Hα and [N II] deblending are also encountered for [S II] λ6717/6731. In this particular case the use of [O III] λ5007 as a shape template was not satisfactory in most cases. As a consequence, we treated all [S II] profiles by a similar technique to the one described in (ii) above. Of course, since no broad component is expected, we simply rectified the local baseline using a straight line, and avoided measurements below the 20 per cent level. Even so, in some cases (e.g. NGC 1052) we should expect greater uncertainties in the profile parameters.

When available, the Hβ profile was treated by a similar procedure to the one outlined in (ii) above.

We also measured, in all possible cases, the equivalent width of each line, separating contributions from the narrow and broad Balmer line components, when appropriate. The continuum used for both broad and narrow components was the same, defined well outside the region occupied by the broad component. In the three cases where sky subtraction was not possible, we measured instead the line ratios against Hα narrow. However, in no case did we attempt to correct the measurements by the underlying stellar contribution, which can be conspicuous in some instances. In objects like NGC 1097 (Phillips *et al.* 1984), the equivalent widths and/or line ratios must be taken as approximations only.

3 RESULTS AND DISCUSSION

The main results are presented in Tables 2–5. Definitions of the profile parameters are presented and discussed in Paper I and references therein. In the tables, *cz* is the line heliocentric radial velocity and S/N is the line signal-to-noise ratio as defined by Vrtilek & Carleton (1985): line peak intensity divided by rms fluctuation on the continuum adjacent to line. Formal errors are shown in parentheses.

Tables 6 and 7 present the line intensity measurements. The order of presentation in all tables goes from objects with dominant broad Balmer component to the ones without it. We note that, due to the higher spectra resolution of our data, when compared with previous work (references in Paper I), we are usually able to assign a more accurate AGN class to each object. These are discussed below, for each individual object, and also summarized in Table 1.

The line deblending process revealed the presence of broad Hα emission in IC 5135 and IC 5063. It also failed to reveal a strong broad component in NGC 2992. These cases were briefly discussed in Busko & Steiner (1989b), and are fully presented below.

In what follows, a discussion of each object is presented.

MKN 926. The recession velocity shifts Hα exactly under the O_2 band at λ6870, completely obliterating it. Therefore, it is not shown in Fig. 1. Although of low signal-to-noise, there are indications that the [S II] lines show the same kind of red asymmetry as found in the [O III] line.

Table 2. Hα narrow component profile parameters.

Object	W80	W50	W20 (km.s^{-1})	W10	AI50	AI20	AI10	cz (km.s^{-1})	S/N
NGC 6814	25(10)	170(35)	330(55)		0.24(.26)	0.21(.20)		1588(9)	11
MCG-6-30-15	77(18)	169(9)	257(11)		-.07(.05)	0.01(.04)		2335(8)	21
F51	68(4)	251(6)	425(27)	540(46)	-.19(.02)	-.20(.05)	-.19(.07)	4211(3)	33
NGC 7213	142(24)	298(40)	560(67)		0.09(.15)	0.00(.12)		1769(17)	7
NGC 1052	201(21)	329(35)	551(20)		0.08(.12)	0.05(.04)		1437(15)	5
NGC 1566	33(4)	181(10)	304(11)		0.34(.08)	0.19(.04)		1540(3)	15
IC 5135	52(6)	146(7)	290(4)	370(8)	-.05(.04)	0.10(.02)	0.10(.02)	4843(4)	133
NGC 5728[a]	210(13)	420(12)	613(17)		0.22(.04)	0.27(.03)		2952(9)	11
IC 5063	148(6)	276(8)	565(19)	850(60)	0.04(.03)	-.04(.03)	0.03(.07)	3370(4)	47
NGC 2992	96(5)	240(20)	503(45)	803(96)	0.27(.10)	0.39(.13)	0.48(.18)	2360(4)	40
Mkn 938	70(8)	264(7)	444(59)		0.22(.03)	0.01(.13)		5844(5)	20
NGC 7552	81(6)	153(6)	251(4)	340(8)	0.09(.04)	0.13(.02)	0.18(.03)	1604(4)	88
NGC 7582	43(5)	145(6)	320(12)	438(15)	0.17(.05)	0.33(.05)	0.35(.05)	1635(4)	122
NGC 6300	125(16)	198(9)	251(8)		-.06(.04)	-.08(.03)		971(12)	5
NGC 1097 n	143(8)	284(34)	460(20)		0.26(.15)	0.21(.05)		1267(6)	5
NGC 1097 1	138(4)	197(7)	306(34)		-.06(.03)	0.10(.12)		1282(3)	10
NGC 1097 2	48(9)	100(6)	215(8)		0.00(.06)	-.07(.03)		1323(6)	12
NGC 253 1	63(9)	175(6)	320(8)	410(21)	0.25(.04)	0.34(.02)	0.30(.07)	226(7)	55
NGC 253 2	103(4)	198(6)	352(7)	432(12)	0.04(.03)	0.05(.02)	0.07(.03)	180(3)	61
NGC 253 3	72(5)	216(6)	298(8)	352(11)	-.26(.02)	-.06(.02)	-.06(.03)	176(4)	23

Note: [a]double-peaked line.

© Royal Astronomical Society • Provided by the NASA Astrophysics Data System

1990MNRAS.245..470B

Table 3. Hβ narrow component profile parameters.

Object	W80	W50	W20 (km.s^{-1})	W10	AI50	AI20	AI10	cz (km.s^{-1})	S/N
MCG-6-30-15	27(21)	104(19)			-.26(.14)			2324(15)	5
F51	180(15)	290(60)	525(240)		-.01(.20)	-.18(.37)	-.19(.86)	4234(11)	6
NGC 1052	210(90)	670(130)			0.45(.30)			1385(65)	5
IC 5135	65(9)	160(5)	353(37)	613(150)	-.07(.03)	0.17(.12)	0.32(.23)	4857(6)	17
IC 5063	290(71)	440(35)	636(75)	820(170)	0.00(.08)	0.00(.11)	0.04(.20)	3394(70)	6
NGC 2992	103(32)	230(62)	605(215)		0.16(.22)	0.25(.27)		2361(32)	30

Table 4. [N II]λ6583 profile parameters.

Object	W80	W50	W20 (km.s^{-1})	W10	AI50	AI20	AI10	cz (km.s^{-1})	S/N
ESO141-G55	140(35)	260(46)	444(87)					11098(25)	2
NGC 6814	87(16)	188(20)	340(30)	460(64)	0.03(.11)	0.04(.09)	0.09(.15)	1561(11)	27
MCG-6-30-15	92(27)	195(19)	258(26)		-.22(.08)	-.19(.09)		2314(20)	9
F51	154(15)	270(13)	417(44)	508(63)	0.00(.05)	-.04(.10)	-.09(.11)	4243(11)	33
NGC 7213	147(18)	292(23)	474(53)		0.07(.09)	0.08(.12)		1768(13)	17
NGC 1052	212(45)	425(37)	648(64)		-.04(.08)	-.06(.09)		1454(32)	7
NGC 1566	25(22)	187(18)	323(17)		0.42(.14)	0.22(.06)		1541(16)	21
IC 5135	73(7)	195(8)	418(19)	566(36)	0.09(.05)	0.16(.05)	0.17(.07)	4831(5)	78
NGC 5728[a]	217(8)	580(12)	813(21)		0.40(.03)	0.32(.03)		2994(6)	18
IC 5063	204(17)	357(12)	570(33)	810(115)	-.10(.03)	-.11(.05)	-.05(.13)	3378(12)	26
NGC 2992	71(6)	186(17)	445(26)		0.15(.10)	0.21(.07)		2346(4)	34
Mkn 938	246(13)	384(12)	610(19)		-.05(.03)	0.02(.03)		5779(9)	19
NGC 7552	74(4)	152(4)	271(7)	365(16)	0.15(.03)	0.13(.03)	0.19(.05)	1601(3)	50
NGC 7582	43(5)	158(8)	351(16)	445(8)	0.26(.07)	0.35(.06)	0.36(.02)	1628(3)	75
NGC 6300	109(10)	232(9)	405(39)	493(31)	-.08(.04)	0.05(.10)	0.03(.07)	1002(6)	12
NGC 1097 n	113(10)	317(23)	481(29)	588(13)	0.14(.08)	0.05(.06)	-.02(.02)	1248(7)	8
NGC 1097 1	84(3)	142(4)	296(13)		0.15(.03)	0.05(.05)		1273(2)	7
NGC 1097 2	61(13)	138(19)			-.15(.12)			1288(9)	8
NGC 253 1	80(7)	205(4)	341(19)	457(18)	0.21(.03)	0.33(.08)	0.37(.05)	213(5)	36
NGC 253 2	92(18)	214(20)	344(8)	446(16)	0.00(.10)	0.03(.02)	0.07(.04)	173(13)	48
NGC 253 3	94(4)	211(12)	328(5)	423(18)	-.15(.05)	-.04(.02)	0.03(.05)	172(3)	16

Note: [a]double-peaked line.

IC 4329A. Very weak emissions of [S II], [N II] and narrow Hα; the profile shapes are not measurable in our spectrum. However, an estimate for the ratio narrow/broad in the Balmer lines allows us to classify this object tentatively as a Seyfert 1–1.2.

NGC 3783 and *ES0141-G55.* A barely visible narrow Hβ component points to a Sy1–1.2 classification for these objects. The Hα exposure for NGC 3783 was lost due to equipment failure.

NGC 6814. Relatively narrow lines, as was already remarked for [O III] λ5007 (Paper I). The Hα broad/narrow ratio is indicative of a Sy 1.2–1.5; also, the ratio [N II]/Hα is relatively high. Albeit noisy, the profiles of the [S II] lines show indications of a susbtantial blue asymmetry, contrary to the other lines.

MCG-6-30-15. Also a case of relatively narrow lines, and intermediate broad/narrow ratio like NGC 6814. In contrast with the uninteresting [O III] profile, both Hα and [N II] λ6583 are flat-topped and show a strong, red asymmetry.

F51. Also an object with narrow profiles and intermediate Seyfert nature. Analogous to MCG-6-30-15, the narrow lines show very different profiles among each other. The asymmetry parameter seems to be correlated with the line critical density.

F9. This object was relatively well studied as regards variability of different spectral components (Morini *et al.* 1986; Wamsteker *et al.* 1985; Kollatschny & Fricke 1985). Although not observed in the Hα region, we found a Hβ broad/narrow ratio within 15 per cent of the value observed by Wamsteker *et al.* 37 days after our observation, so the errors in our broad/narrow ratios could be of this order.

NGC 7213. Apart from the remarkable [O III] profile discussed in Paper I, this object shows more normal looking profiles on the other observed lines. Also, an intermediate Sy 1.2–1.5 can be assigned to it, albeit its LINER nature. As we did with the [O III] profile, the measured spectrum is the raw one, without sky subtraction, due to noticeable contamination of the detector sky channel by galaxy light.

NGC 1052. Also a well known LINER prototype, shows a similar spectrum to NGC 7213, although with still broader lines. The parameters derived for the [S II] lines must be regarded with caution, due to their strong blending.

NGC 1566. A well-known variable Hα object (Alloin *et al.* 1986, 1985). Our spectrum shows a weak broad component (Sy 1.9), suggesting that the object was in a minimum at the time. Both Hα and [N II] λ6583 show correlated multi-component structure.

© Royal Astronomical Society • Provided by the NASA Astrophysics Data System

1990MNRAS.245..470B

Table 5. [S II]λ6717/6731 profile parameters.

Object[a]	W80	W50	W20 (km.s^{-1})	W10	AI50	AI20	AI10	cz (km.s^{-1})	S/N
Mkn 926	257(110)	445(127)	700(210)		-.13(.24)	-.20(.23)		14057(81)	4
	242(30)	410(122)			-.19(.23)			14039(21)	3
NGC 6814	39(21)	174(48)	440(130)		0.07(.30)	0.13(.33)		1560(15)	5
	106(29)	217(36)	390(150)		-.07(.15)	0.19(.47)		1552(21)	6
MCG-6-30-15	49(10)	168(16)	241(20)		-.36(.06)	-.23(.06)		2307(7)	6
	118(26)	206(32)	302(34)		-.06(.15)	-.10(.10)		2308(18)	4
F51	150(11)	218(19)	340(33)		-.07(.04)	-.16(.08)		4206(8)	6
	157(28)	260(20)	455(140)		0.05(.09)	-.06(.29)		4230(20)	5
NGC 7213	125(24)	257(32)	582(103)		0.02(.13)	0.00(.18)		1770(17)	7
	175(32)	287(18)			0.07(.07)			1753(23)	6
NGC 1052	295(23)	420(52)	590(82)		0.04(.13)	0.22(.17)		1426(16)	8
	215(52)	440(56)			-.04(.12)			1435(37)	4
NGC 1566	104(9)	219(11)	308(26)		-.13(.04)	0.12(.08)		1483(7)	5
	202(8)	248(6)	322(21)		0.03(.03)	0.17(.07)		1479(5)	4
IC 5135	76(17)	186(28)	410(102)		0.14(.17)	0.39(.34)		4845(12)	13
	104(25)	295(45)	638(57)		0.19(.18)	0.37(.12)		4818(18)	9
IC 5063	223(42)	414(30)	640(59)		-.13(.06)	-.12(.08)		3392(30)	10
	175(31)	365(26)	690(75)		-.10(.06)	0.06(.11)		3391(22)	10
NGC 2992	146(27)	285(30)	490(57)		0.14(.12)	0.14(.13)		2323(19)	11
	85(16)	212(20)	425(69)		0.04(.10)	0.03(.17)		2340(11)	10
Mkn 938[b]	132(50)	308(83)			0.22(.33)			5830(35)	5
NGC 7552	119(19)	192(21)	326(66)		0.09(.12)	0.20(.24)		1576(14)	7
	98(10)	152(4)	240(24)		-.08(.02)	0.08(.11)		1585(7)	10
NGC 7582	64(17)	206(28)	383(41)		0.29(.18)	0.38(.15)		1614(12)	15
	82(10)	214(14)	405(48)		0.15(.07)	0.41(.17)		1606(22)	16
NGC 6300	84(36)	235(29)	400(65)		0.34(.17)	0.47(.24)		1021(25)	3
NGC 253 1	48(13)	173(16)	320(33)		0.19(.11)	0.20(.13)		174(10)	9
	134(11)	236(18)			0.09(.08)			168(7)	7
NGC 253 2	108(7)	224(16)	382(28)		0.06(.08)	0.06(.08)		153(5)	15
	129(6)	224(4)	350(10)		-.04(.02)	-.01(.03)		154(5)	11

Notes: [a]First line of each object: λ6717; second line: λ6731; [b]λ6731 affected by O_2 band at 6870 Å.

Table 6. Equivalent widths (in Å) of emission lines.

Object	Hα (n)[a]	Hα (b)	Hβ (n)	Hβ (b)	[OIII] λ5007	[NII] λ6583	[SII] λ6717	[SII] λ6731
Mkn 926			6.4	412	40			
IC 4329A	17	470	<2.7	88	36	~9	2.3	2.2
NGC 3783			4.7	110	103			
ESO141-G55		330	~2	48	18			
NGC 6814	8	110			20	16	4.5	4.5
MCG-6-30-15	11	145	2.2	31	19	4.2	2.3	~1.6
F51	21	250	6.6	66	43	11	4	3
F9			3.8	41	31			
NGC 1052	~3	25	4.3		11	8	~11	~9
NGC 1566	9.9	21				12	3.4	3.4
IC 5135	72	125[b]	12		71	70	12	10
NGC 5728	32	~45				51		
IC 5063	54	39	14		163	35	19	15
NGC 2992	35	<8	7.5		80	43	14	12
Mkn 938	23					28	5.7	
NGC 7552	48					30	6.3	5.6
NGC 7582	94					62	14	15
NGC 6300	4.3					13	3	~1

Notes: [a]narrow (n) and broad (b) components shown separately; [b]Hβ profile for deblending. When using a composite profile derived from the [S II] lines, east–west becomes ~ 75 Å.

IC 5135. A most interesting object, in which great differences are seen amongst the profiles of different lines. Two spectra were secured on different dates. Both were rebinned to a common wavelength scale and co-added, since no differences beyond those expected from counting statistics were found beween them.

As pointed out in Paper I, [O III] λ5007 shows a particularly 'fat' profile. This prevented using it as a template for line deblending. Instead, Hβ was used. When removing [N II] λ6583 and λ6548 by the method outlined in Section 2 above, a weak (equivalent width ~ 125 Å), broad (FWZI ~ 3000 km s^{-1}), nearly Gaussian residual remains on the spectrum (Fig. 2a). To check further the reality of this broad component, we repeated the deblending procedure, using as template the profile of [S II] λ6717/6731. Since these lines are blended themselves, the actual template was built up by joining the blue wing of λ6717 with the red wing of λ6731. We included in this composite profile the broad base shown by the [S II] lines, particularly conspicuous to the blue side of λ6717. The reasoning behind this is that, if the broad residual seen in the Hα region after deblending is due only to broad wings present in the [N II] lines (and *not* present in Hβ), it must disappear, or at least be susbtantially reduced, when a template with similar broad wings is used for the

© Royal Astronomical Society • Provided by the NASA Astrophysics Data System

1990MNRAS.245..470B

Table 7. Emission-line intensity ratios [H$\alpha(n) = 1.00$].

Object	Hα(b)[a]	[NII] λ6583	[SII] λ6717	[SII] λ6731
NGC 7213	9.57	1.69	0.44	0.64
NGC 1097 n		1.88		
NGC 1097 1		0.53		
NGC 1097 2		0.71		
NGC 253 1		0.80	0.15	0.15
NGC 253 2		0.82	0.20	0.17
NGC 253 3		0.78	0.21	0.19

Note: [a]broad component.

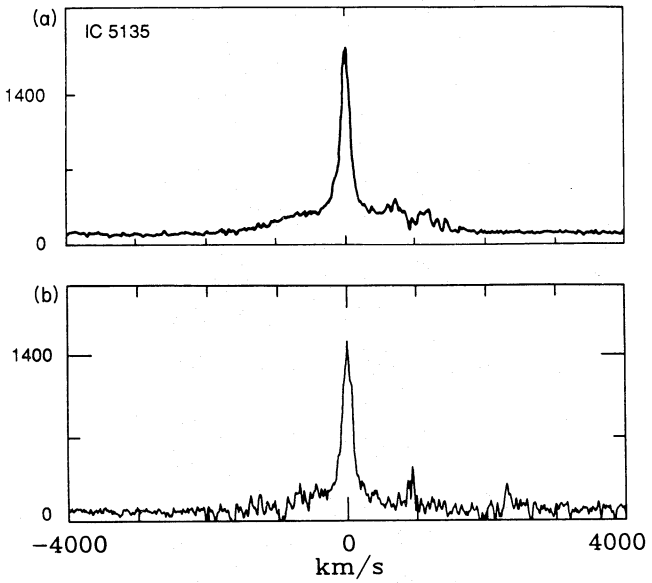

Figure 2. (a) Hα emission-line profile of IC 5135, after deblending by Hβ template. (b) same as (a), but using as template a composite profile obtained from [S II] λ6717/6731. Abscissa: velocity (in km s^{-1}) in the object reference frame. Ordinate: total counts per 10 km s^{-1} velocity bin.

deblending. Instead, a similar broad residual still remains after this deblending. Fig. 2(b) shows the result, with a broad component with equivalent width ~ 75 Å, FWZI ~ 3500 km s^{-1}.

It can always be argued that the template was not a good one; this argument is particularly true in an object like this, in which so great profile differences are seen between different emission lines. Clearly, a more complete spectral coverage in high resolution is needed to confirm the reality of this broad Hα component.

NGC 5728. Very broad and complex profiles are shown by the Hα and [N II] lines. Double peaked structure can be seen in both lines, possibly due to a shell-structured emission region. The [N II]/Hα ratio is relatively high. Unfortunately, profile information on the [S II] lines is rendered useless by the very low signal-to-noise ratio.

IC 5063. This is a well-known radio source (PKS2048 – 57), showing also IR emission and optical–IR polarization (Hough *et al.* 1987, Axon, Bailey & Hough 1982). Emission line nebulosity is found in a large region around the nucleus (Caldwell & Phillips 1981; Bergeron, Durret & Boksenberg 1983).

After removing the [N II] profiles from the Hα region, a weak (equivalent width ~ 40 Å), broad (FWZI ~ 4000 km s^{-1}) component remains (Fig. 3a). This component had already been detected by Bergeron *et al.* (1983), with similar broad/narrow ratio to ours (0.72).

The lines in this object have a marked multi-component appearance, including flat tops and double peaks. We attempted to describe these profiles by multiple Gaussians, assuming that 'cloud ensembles' with differentiated dynamics and structure are responsible for them. Under this assumption, we should expect that each Gaussian component found in one given line must have a corresponding component (in velocity space) in the other lines as well. The multiple Gaussians were fitted to each profile by minimization of the residuals sum-of-squares by the downhill simplex method. The number of components was kept to a minimum: two for the narrow line, plus one broad and shallow component. We tried to restrict the positions of the narrower components so as not to deviate more than a few tens of km s^{-1} from the line centre, since good fits can also be obtained with very narrow (FWHM ~ 100 km s^{-1}) components situated far away (> 200 km s^{-1}) from the line centre. These are, however, physically less realistic situations, although resulting in fits with similar or even slightly better formal quality.

The profiles of both deblended Hα and [O III] λ5007 are reasonably well fit by that set of components. The results can be seen in Fig. 3 and Table 8. Both components 1 and 2 show some degree of correspondence in position and FWHM between Hα and [O III]. The same cannot be said in relation to component 3, however, indicating that 'broad' [O III] λ5007 and broad Hα must be produced in regions with distinct velocity structure. We cannot rule out the hypothesis that at least part of the broad Hα emission is related to [O III] component number 3.

In both [N II] λ6583 and Hβ, we were unable to find more than one detectable component. However, our data do not rule out the existence of a possible broad and shallow component in [N II] λ6583, associated with component 3 in [O III] λ5007. In order to derive upper limits to line ratios, we forced in both cases a two-component fit, with the relative positions and FWHM pre-fixed with values taken from the corresponding Hα and [O III] λ5007 components. The results are summarized in Table 8. We can see that each narrow component shows different excitation characteristics, which we can interpret as indication of an excitation-structured emission line region.

Component 3 in [O III] λ5007 could be associated to a 'transition zone' emission, as proposed by van Groningen & de Bruyn (1989). As pointed out by Kennicutt, Kel & Blaha (1989), many galaxies show composite nuclei, that is, superposition of nuclear line emission due to both stellar and non-stellar excitation sources. When observed with sufficient spectral resolution, as in the present case, these nuclei perhaps show their composite nature on the line profiles themselves.

NGC 2992. A well-studied object in what regards the [O III] λ5007 line. Apart from the studies cited in Paper I, long-slit observations of this line by Colina *et al.* (1987) point to a complex, spatially extended emission line region. Common to all spectral lines observed by us, the very

© Royal Astronomical Society • Provided by the NASA Astrophysics Data System

1990MNRAS.245..470B

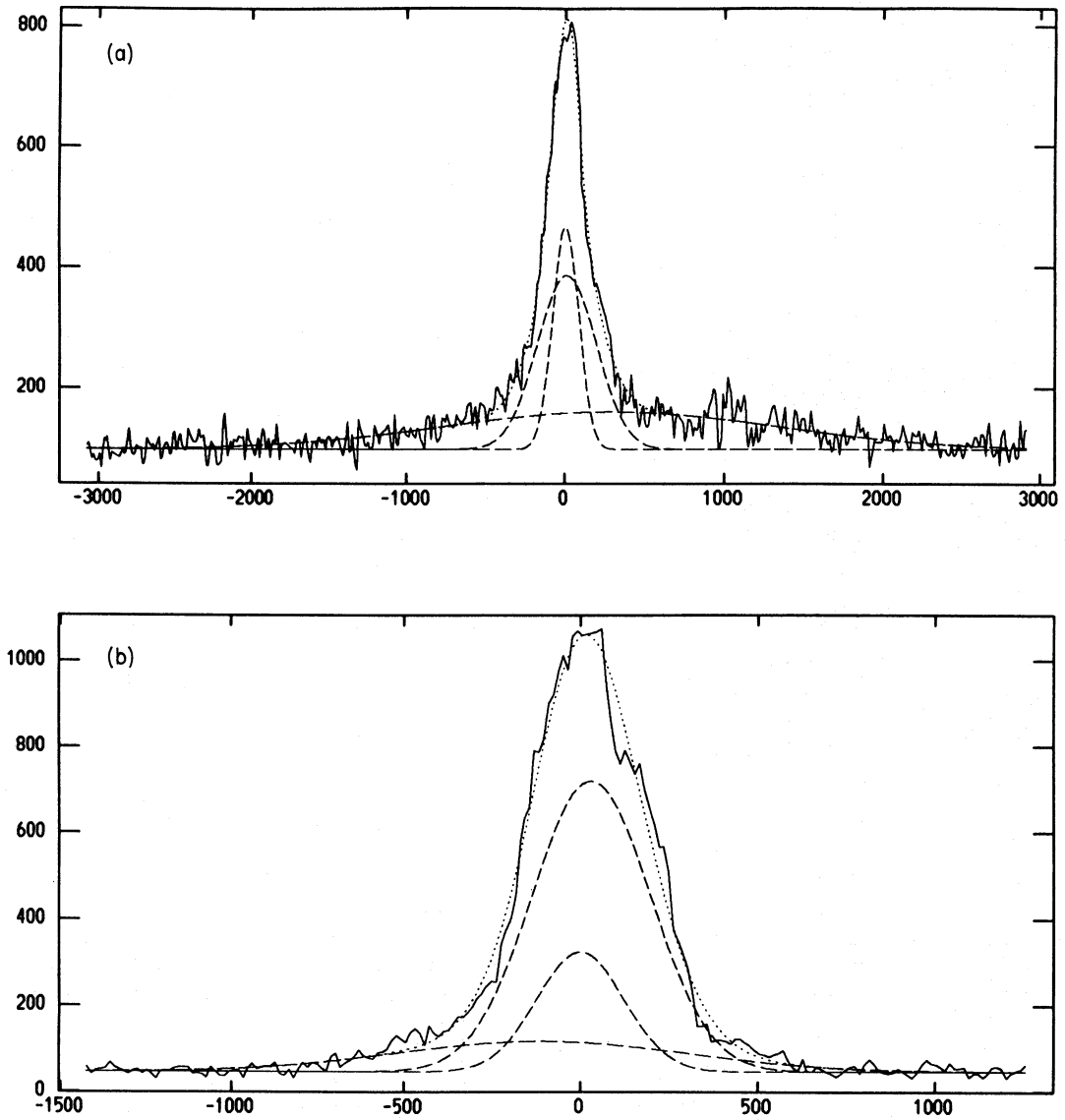

Figure 3. Line profiles of IC 5063: (a) Hα, after deblending by [O III] λ5007 template; (b) [O III] λ5007. Abscissa: velocity (in km s^{-1}) in the object reference frame. Ordinate: total counts per 10 km s^{-1} velocity bin. The dashed lines are Gaussian components (see text).

Table 8. Gaussian decomposition of profiles in IC 5063.

Component	E.W. (Å)	Position[a] (km.s^{-1})	FWHM (km.s^{-1})	Intensity ratio
[OIII] 1	29 (8)[c]	-1 (02)	280 (14)	>30
[OIII] 2	95 (12)	30 (08)	390 (18)	7 (3)
[OIII] 3	24 (15)	-115 (10)	950 (05)	
Hα 1	17 (02)	2 (03)	195 (08)	
Hα 2	28 (03)	14 (04)	430 (15)	
Hα 3	35 (05)	270 (20)	2460 (40)	
[NII]λ6583 1	3 (03)	2[b]	195[b]	0.2 (0.2)
[NII]λ6583 2	22 (05)	14[b]	430[b]	0.8 (0.2)
Hβ 1	<1	-1[b]	280[b]	
Hβ 2	13 (02)	30[b]	390[b]	

Notes: [a]relative to cz as given in Tables 2, 3, 4 and Table 2 of Paper I; [b]pre-fixed before fit (see text); [c]standard errors in parentheses.

conspicuous blue asymmetry and narrow core stand out clearly. Also, the object shows relatively strong [N II] lines.

The Hα profile was previously studied by Shuder (1980) and Ward *et al.* (1980) using a lower resolution (5 Å). After removing the [N II] lines by a similar process to the one used in the present work, they found a strong broad Hα component, with intensity similar to the narrow Hα intensity ($b/n=1.23$, Ward *et al.* 1980; $b/n=0.9$, Shuder 1980). We were, however, unable to detect a component that strong. Any broad component in our spectrum, after removal of both narrow Hα and [N II], must have an intensity no more than 20 per cent of the narrow component.

What is the reason for such a discrepancy? One could argue that the difference in flux is real, perhaps caused by variability of the broad component, or, alternatively, by slightly different slit positioning during the observations. There is a third possibility, which is perhaps the most

© Royal Astronomical Society • Provided by the NASA Astrophysics Data System

1990MNRAS.245..470B

plausible explanation. The previous authors used a much lower resolution than we did. The effect is dramatic as regards the widths measured for the narrow lines. Shuder quotes FWHM of 450 km s^{-1} for Hα and ~330 km s^{-1} for the other narrow lines. Contrast this with the smaller values found by us and other authors (in this work and Paper I). Also, since the lines are strongly asymmetric, the deblending at low reslution is a delicate task. To test the effect of resolution on the result of the deblending, we degraded numerically our original spectra to 4.7 Å (both Hα and [O III]), and repeated the deblending procedure. The result is shown in Fig. 4. The broad/narrow ratio on the degraded spectrum is ~1, about five times larger than the ratio obtained with full resolution, and in accordance with previous authors.

Mkn 938. Structured and complex profiles, with great differences in width and shape between Hα and [N II] λ6583. The [S II] λ6731 profile is obliterated by atmospheric O_2.

NGC 7552 and *NGC 7582.* Two objects with several characteristics in common. The host galaxies are probably physically associated; neither shows broad Balmer line emission; very bright and narrow lines, with similar intensity ratios in both objects. Both show the classic blue asymmetry in the line profiles; however, the degree of asymmetry is very different between them.

NGC 6300. Profiles of Hα and [N II] λ6583 are symmetrical, in accordance with the [O III] profile published by Phillips, Charles & Baldwin (1983). The abnormal λ6717/λ6731 ratio is probably due to the intrinsic weakness of the lines, coupled to the presence of a stellar continuum.

NGC 1097. This is a well-known case of circumnuclear 'ring' line emission, relatively well-studied at radio, optical and UV wavelengths (Hummel, van der Hulst & Keel 1987; Walsh *et al.* 1986; Phillips *et al.* 1984). We observed this object on two different nights; the resulting nuclear spectra were co-added after being rebinned to a common wavelength scale. However, since there was also emission on the detector sky channel, we did not subtract the sky from the object channel; instead, we treated it as a second object. Since different sky regions were observed on each night (due to the coudé focal plane rotation), we ended up with three different spectra. They are shown in Fig. 5. Regions labelled 1 and 2, resulting from the arc traced on the sky by the rotating sky slit, are shown, in Fig. 6, superimposed on a sketch of the emission region. We note that the spectrograph sky slit, being at a fixed distance from the object slit, unfortunately just missed the region of stronger Hα emission. Nevertheless, a detectable Hα signal was present on the sky channel. No [S II] emission is detectable in any of our spectra.

We find a good degree of correlation between our nuclear spectrum and the one of lower resolution (65 km s^{-1}) published by Phillips *et al.* (1984). However, it must be emphasized that our spectrum is not decontaminated from the effects of the underlying stellar absorption spectrum; the results must be taken with caution. In the extra-nuclear regions there is evidence of much dynamical structure, with the line profile shapes varying between regions 1 and 2. In particular, region 1 shows evidence of shell-like movements, pointing to a possible torus structure for the ring of emission, as pointed out by Hummel *et al.* (1989).

NGC 253. This is a well-known starburst nucleus (Turner & Ho 1983), showing several point-like X-ray sources (Fabbiano & Trinchieri 1984). We looked for detectable line emission at all positions listed in Fabbiano & Trinchieri's table 1. We also did a systematic scan over a region 15 × 15 $arcsec^2$ centred on the radio nucleus positioned obtained from the 2-cm map of Turner & Ho. The region was explored by integrating with the double slit in seven positions separated by 2 arcsec in the direction perpendicular to slit length, and repeating the sequence with the slits moved 5 arcsec in the direction of their length. The slits were held fixed in each position for 5–8 min, and the resulting data were used to estimate how much integration time would be necessary to get an exposure with a good signal-to-noise ratio.

No emission suitable for obtaining a useful spectrum was detected in any of the X-ray positions. We found, however, extended weak line emission all around the radio nucleus, and three regions with strong enough Hα emission to guarantee a good spectrum: the radio nucleus itself (position no. 1), a spot 10 arcsec east of it with the strongest emission among all the explored positions (no. 2), and another one 3 arcsec east of the radio nucleus (no. 3). The corresponding spectra are shown separately in Fig. 1. Excitation conditions seem to

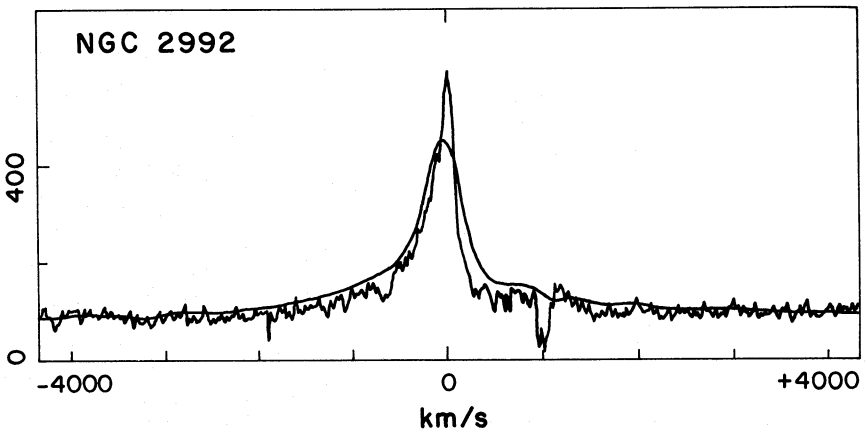

Figure 4. Deblended Hα profile of NGC 2992. The smooth line is the result of deblending after degrading numerically the original resolution (0.6 Å) to 4.7 Å. Abscissa: velocity (in km s^{-1}) in the object reference frame. Ordinate: total counts per 10 km s^{-1} velocity bin.

© Royal Astronomical Society • Provided by the NASA Astrophysics Data System

1990MNRAS.245..470B

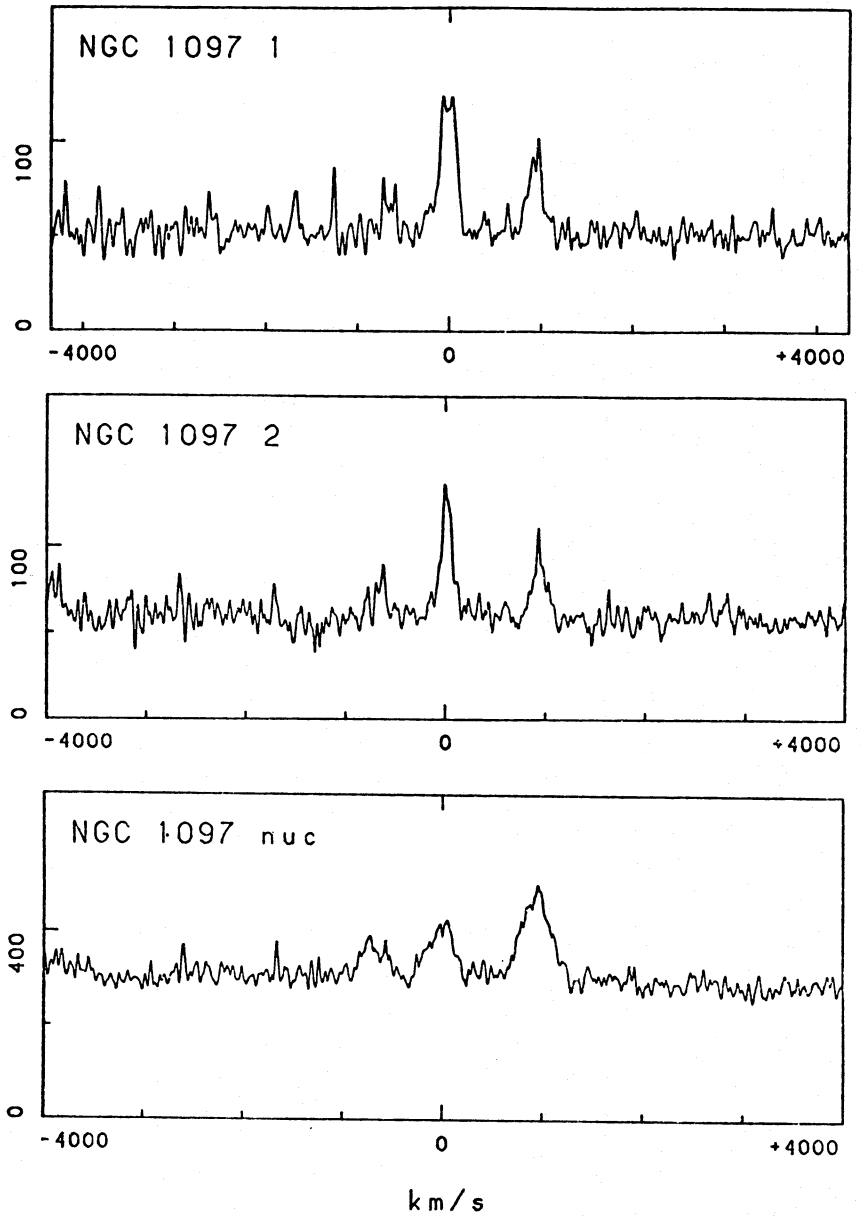

Figure 5. Hα and [N II] emission-line profiles in NGC 1097. Spectra labelled 1 and 2 came from the regions shown in Figure 6. Abscissa: velocity (in km s^{-1}) in the object reference frame. Ordinate: total counts per 10 km s^{-1} velocity bin.

be similar in the three regions, but the profile shapes are substantially different, showing a great degree of complexity in the region's structure, with predominance of shell-like emission. Clearly, long-slit spectroscopy of this object is needed.

4 CONCLUSIONS

In this paper, we present high-resolution narrow emission line profiles of Hα, [N II] λ6583/6548 and [S II] λ6717/6731, for several southern AGN. The profiles were measured following the set of descriptor parameters introduced by Heckman *et al.* (1981). Also, equivalent widths and/or line ratios were measured not only for the narrow lines, but also for the broad Balmer components, when present.

We found the presence of structure in the line cores, in the form of multiple peaks or flat-topped lines, pointing to the dynamical complexity present in the low-velocity regions of the NLR. Also, the diversity of narrow line profile shapes amongst the different objects, as well as among different lines of the same object, is conspicuous. Nevertheless, profile deblending using the [O III] λ5007 (when available) as shape template for the [N II] and narrow Hα lines, was relatively successful.

In IC 5063, a profile description by multiple Gaussians shows that the emission lines are produced in regions with different excitation conditions. In particular, evidence for a possible high-ionization 'transition zone' is found in this object.

We found evidence of a weak, broad Hα component in IC 5063, as previously reported by Bergeron *et al.* (1983),

© Royal Astronomical Society • Provided by the NASA Astrophysics Data System

1990MNRAS.245..470B

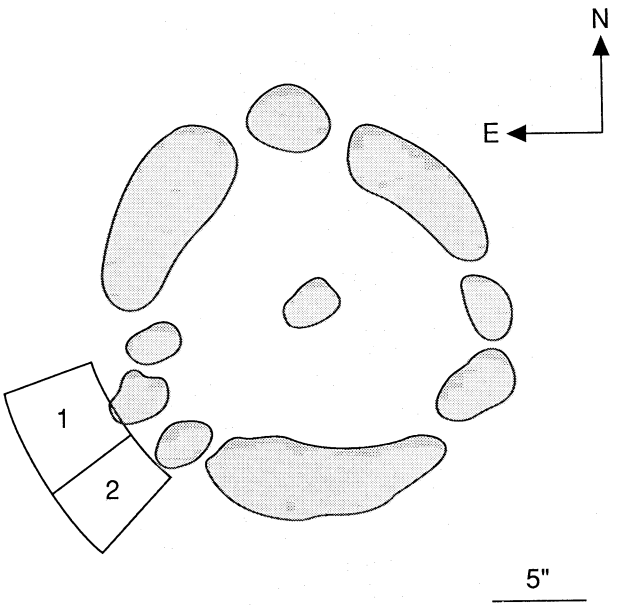

Figure 6. Sketch of the emitting region in NGC 1097, showing the two areas swept by the coudé spectrograph sky channel.

and also in IC 5135. However, in this last object the detection is more controversial, due to the very different profile shapes found in different lines. We were unable to detect a broad Hα component in NGC 2992 with broad/narrow ratio ~ 1, as reported by previous authors. Instead, our detection points to a value closer to 0.2 for the same ratio. The explanation could be variability and/or slit effects, or, most probably, a spectral resolution effect.

ACKNOWLEDGMENTS

Part of this work was done with support from Fundação de Amparo à Pesquisa do Estado de São Paulo, under grant no. 88/1011-2. ICB acknowledges the Space Telescope Science Institute for its hospitality.

REFERENCES

Alloin, D., Pelat, D., Phillips, M. M. & Whittle, M., 1985. *Astrophys. J.*, **288,** 205.
Alloin, D., Pelat, D., Phillips, M. M., Fosbury, R. A. E. & Freeman, K., 1986. *Astrophys. J.*, **308,** 23.
Appenzeller, I. & Östricher, R., 1988. *Astr. J.*, **95,** 45.
Axon, D. J., Bailey, J. & Hugh, J. H., 1982. *Nature*, **299,** 234.
Ayani, K. & Iye, M., 1989. *Astr. J.*, **97,** 3.
Bergeron, J., Durret, F. & Boksenberg, A., 1983. *Astr. Astrophys.*, **127,** 322.
Busko, I. C. & Steiner, J. E., 1988. *Mon. Not. R. astr. Soc.*, **232,** 525 (Paper I).
Busko, I. C. & Steiner, J. E., 1989a. *Mon. Not. R. astr. Soc.*, **238,** 1479 (Paper II).
Busko, I. C. & Steiner, J. E., 1989b. *Active Galactic Nuclei, IAU Symp. No. 134,* p. 90, eds Osterbrock, D. E. & Miller, J. S., Kluwer Academic Publishers, Dordrecht.
Buta, R., 1987. *Astrophys. J. Suppl.*, **64,** 383.
Caldwell, N. & Phillips, M. M., 1981. *Astrophys. J.*, **244,** 447.
Colina, L., Fricke, K. J., Kollatschny, W. & Perryman, M. A. C., 1987. *Astr. Astrophys.*, **178,** 51.
Fabbiano, G. & Trinchieri, G., 1984. *Astrophys. J.*, **286,** 491.
Heckman, T. M., Miley, G. K., van Breugel, W. J. M. & Butcher, H. R., 1981. *Astrophys. J.*, **247,** 403.
Hough, J. H., Brindle, C., Axon, D. J., Bailey, J. & Sparks, W. B., 1987. *Mon. Not. R. astr. Soc.*, **224,** 1013.
Hummel, E., van der Hulst, J. M. & Keel, W. C., 1987. *Astr. Astrophys.*, **172,** 32.
Kennicutt, R. C., Keel, W. C. & Blaha, C. A., 1989. *Astr. J.*, **97,** 1022.
Kollatschny, W. & Fricke, K. J., 1985. *Astr. Astrophys.*, **146,** L11.
Morini, M., Scarsi, L., Molteni, D., Salvati, M., Perola, G. C., Piro, L., Simari, G., Boksenberg, A., Penston, M. V., Snijders, M. A. J., Bromage, G. E., Clavel, J., Elvius, A. & Ulrich, M. H., 1986. *Astrophys. J.*, **307,** 486.
Phillips, M. M., Charles, P. A. & Baldwin, J. A. 1983. *Astrophys. J.*, **266,** 485.
Phillips, M. M., Pagel, B. E. J., Edmunds, M. G. & Díaz, A., 1984. *Mon. Not. R. astr. Soc.*, **210,** 701.
Shuder, J. M., 1980. *Astrophys. J.*, **240,** 32.
Turner, J. L. & Ho, P. T. P., 1983. *Astrophys. J.*, **268,** L79.
van Groningen, E. & de Bruyn, A. G., 1989. *Astr. Astrophys.*, **211,** 293.
Vrtilek, J. M. & Carleton, N. P., 1985. *Astrophys. J.*, **294,** 106.
Walsh, J. R., Nandy, K., Thompson, G. I. & Meaburn, J., 1986. *Mon. Not. R. astr. Soc.*, **220,** 453.
Wamsteker, W., Alloin, D., Pelat, D. & Gilmozzi, R., 1985. *Astrophys. J.*, **295,** L33.
Ward, M., Penston, M. V., Blades, J. C. & Turtle, A. J., 1980. *Mon. Not. R. astr. Soc.*, **193,** 563.
Whittle, M., 1985a. *Mon. Not. R. astr. Soc.*, **213,** 1.
Whittle, M., 1985b. *Mon. Not. R. astr. Soc.*, **216,** 817.

© Royal Astronomical Society • Provided by the NASA Astrophysics Data System